Inorganic Chemistry
Article
Cite This: Inorg. Chem. XXXX, XXX, XXX−XXX
pubs.acs.org/IC

Comparative Study of the Electronic Structures of μ-Oxo, μ-Nitrido, and μ-Carbido Diiron Octapropylporphyrazine Complexes and Their Catalytic Activity in Cyclopropanation of Olefins

Lucie P. Cailler,[†] Martin Clémancey,[§] Jessica Barilone,[§,‡] Pascale Maldivi,*[,‡] Jean-Marc Latour,*[,§] and Alexander B. Sorokin*[,†]

[†]Institut de Recherches sur la Catalyse et l'Environnement de Lyon IRCELYON, UMR 5256, CNRS - Université Lyon 1, 2 avenue A. Einstein, 69626 Villeurbanne cedex, France

[‡]Univ. Grenoble-Alpes, CEA, CNRS, IRIG, CBM, Grenoble 38000, France

[§]Univ. Grenoble-Alpes, CEA, CNRS, IRIG-SyMMES, Grenoble 38000, France

Supporting Information

ABSTRACT: The electronic structure of three single-atom bridged diiron octapropylporphyrazine complexes $(FePzPr_8)_2X$ having Fe(III)−O−Fe(III), Fe(III)−N−Fe(IV) and Fe(IV)−C−Fe(IV) structural units was investigated by Mössbauer spectroscopy and density functional theory (DFT) calculations. In this series, the isomer shift values decrease, whereas the values of quadrupole splitting become progressively greater indicating the increase of covalency of Fe-X bond in the μ-oxo, μ-nitrido, μ-carbido row. The Mössbauer data point to low-spin systems for the three complexes, and calculated data with B3LYP-D3 show a singlet state for μ-oxo and μ-carbido and a doublet state for μ-nitrido complexes. An excellent agreement was obtained between B3LYP-D3 optimized geometries and X-ray structural data. Among $(FePzPr_8)_2X$ complexes, μ-oxo diiron species showed a higher reactivity in the cyclopropanation of styrene by ethyl diazoacetate to afford a 95% product yield with 0.1 mol % catalyst loading. A detailed DFT study allowed to get insight into electronic structure of binuclear carbene species and to confirm their involvement into carbene transfer reactions.

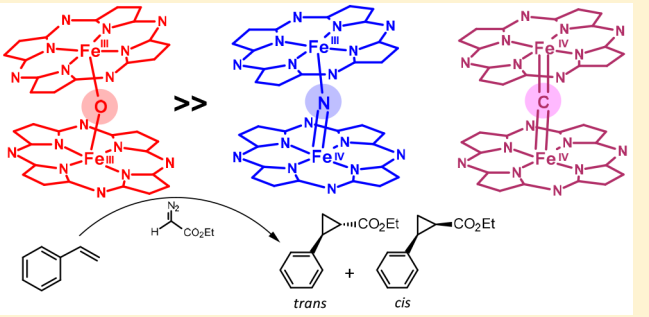

INTRODUCTION

For a long time, research in biomimetic oxidation and related reactions has been associated with mononuclear metal macrocyclic[1,2] and nonheme[3,4] complexes. As for binuclear catalysts, diiron nonheme complexes have attracted significant attention as possible biomimetic catalysts for challenging mild oxidation of methane.[5] Diiron species supported by nonheme scaffolds were also shown to be efficient catalysts for nitrene transfer reactions.[6,7] Since 2000, there is growing evidence that macrocyclic complexes with two single-atom bridged iron sites exhibit interesting catalytic properties in many reactions. These complexes bear two iron sites supported by phthalocyanine, porphyrin, or porphyrazine ligands which can be connected by μ-oxo, μ-nitrido, and μ-carbido bridges.[8] The nature of the bridging group determines the iron oxidation state. Thus, neutral μ-oxo, μ-nitrido, and μ-carbido dinuclear complexes are Fe(III)(μ-O)Fe(III), Fe(III)(μ-N)Fe(IV), and Fe(IV)(μ-C)-Fe(IV) systems. These complexes can be oxidized or reduced to attain other oxidation states.[8] μ-Oxo diiron phthalocyanines were found to catalyze the oxidation of aromatic compounds to corresponding quinones.[9,10] In turn, μ-nitrido diiron macrocyclic complexes have emerged as effective catalysts[11,12] for the oxidation of methane,[13−15] ethane,[16,17] alkanes,[18,19] aromatic compounds,[20] hydroacylation of olefins[21] as well as for oxidative defluorination[22] and dechlorination[23] of halogenated compounds. Although the catalytic activity of μ-carbido diiron species has not been published yet, related μ-carbido diruthenium phthalocyanine catalyzed cyclopropanation of olefins and N−H bonds.[24]

In all these reactions, the electroinsertion of carbene to aminenic structures of the iron complexes and their changes during catalysis play an essential role. In this context, nature and properties of the macrocyclic ligand as well as bridging atom can influence the electronic state and catalytic properties of the single-atom bridged diiron species. In order to discern the structural and electronic differences, a series of the diiron phthalocyanine complexes $(FePc)_2X$ (X = C, N, O) has been investigated by X-ray absorption and emission spectroscopies combined with density functional theory (DFT) calculations.[25] The low-spin μ-nitrido dimer $(FePc)_2N$ has the highest Fe−X bond order, whereas $(FePc)_2C$, a closed-shell structure with Fe=C double bonds, exhibits lower covalency of bridging unit. The Fe−X distances change in the sequence Fe−O > Fe−

Received: September 10, 2019

DOI: 10.1021/acs.inorgchem.9b02718
Inorg. Chem. XXXX, XXX, XXX−XXX

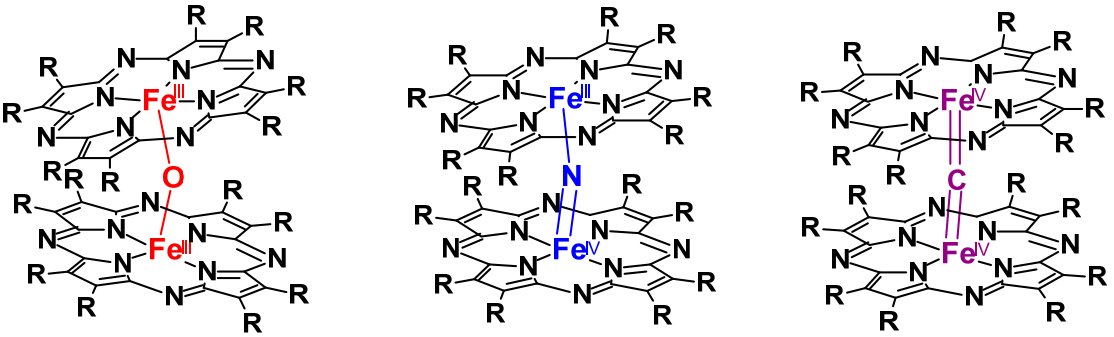

Fe-μX distance	1.750, 1.760 Å	1.656, 1.662 Å	1.669, 1.671 Å
Fe out of plane distance	0.336, 0.367 Å	0.283, 0.291 Å	0.214, 0.219 Å
Fe-X-Fe angle	158.5°	168.5°	175.1°
Staggering angle	24.2°	26.2°	24.2°
Dihedral angle between two Pz planes	19.3°	11.5°	8.2°

Figure 1. Structures of μ-oxo, μ-nitrido, and μ-carbido diiron octapropylporphyrazines complexes used in this study. R = $-CH_2CH_2CH_3$.

C > Fe−N. The most electron-rich μ-oxo complex forms a single Fe−O bond, whereas μ-carbido unit has too high energy of p-electrons and donates them to iron sites. The nature of tetrapyrrolic macrocycle also influences the Mössbauer parameters. Thus, the values of isomeric shift δ in $[LFe(IV)]_2C$ series are −0.04 and 0.10 mm s^{-1} for $(FePc)_2C$ and $(FeTPP)_2C$, respectively.[26]

In continuation of our research project on the catalytic activity of single-atom bridged dimeric macrocyclic complexes, we explore the catalytic properties of μ-oxo, μ-nitrido, and μ-carbido diiron complexes supported by porphyrazine ligand; X-ray structures of which were previously determined (Figure 1).[27]

Noteworthy, the catalytic properties of porphyrazine complexes including their μ-oxo, μ-nitrido, and μ-carbido dimers have been rarely investigated[28] compared to their porphyrin[1,2] and phthalocyanine counterparts.[11,12] One representative example is the oxidation of hydrocarbons by PhIO, iodosylbenzene sulfate, and $KHSO_5$ catalyzed by μ-oxo diiron(III) octakis(perfluorophenyl)tetraazaporphyrin.[29]

In the present work, μ-oxo, μ-nitrido, and μ-carbido diiron octapropylporphyrazine complexes, $(FePzPr_8)_2X$ (X = O, N, C), were evaluated in the reactions of the carbene insertion to the double bond of olefins which has emerged as well-established synthetic approach to cyclopropyl compounds.[30,31] Many transition-metal macrocyclic compounds activate carbene precursors to form putative metal-carbene intermediates which transfer carbenes to olefinic double bonds,[32,33] including preparation of chiral compounds.[34−37] Porphyrin[38,39] complexes of iron,[40−43] cobalt,[44,45] ruthenium,[46,47] iridium,[48] osmium,[31] and rhodium[49] are by far the most studied catalysts in these reactions. Iron and rhodium corrole complexes are also efficient catalysts for the cyclopropanation of olefins.[50]

In sharp contrast, the studies of other tetrapyrrolic catalysts for the preparation of cyclopropane derivatives are scarce. Mononuclear metal phthalocyanine complexes of Cu, Fe, Mn, Ni, Co, Ag, Zn, and Ru were evaluated in the cyclopropanation of styrenes.[51−53] Binuclear single-atom bridged phthalocyanine complexes recently introduced as efficient catalysts for the oxidation and other reactions[11,12] have never been used as the catalysts for cyclopropanation except one case. μ-Carbido diruthenium phthalocyanine in combination with ethyl diazoacetate (EDA) was shown to catalyze cyclopropanation of olefins and insertion of carbene to amine N−H bonds.[24] To the best of our knowledge, the catalytic properties of porphyrazine complexes have never been investigated in carbene transfer reactions. Herein, we evaluate the catalytic properties of μ-oxo, μ-nitrido, and μ-carbido diiron porphyrazine complexes in the cyclopropanation of olefins with ethyl diazoacetate. Detailed Mössbauer studies and DFT calculations provide an insight into electronic structures of these complexes. The electronic structures of the three putative carbene diiron complexes were theoretically characterized for the first time, and their influence on the reactivity in the cyclopropanation of styrenes is discussed.

EXPERIMENTAL SECTION

Materials. Ethyl diazoacetate containing ∼13 wt % of dichloromethane was purchased from Sigma-Aldrich. Iron octapropylporphyrazine and its μ-oxo, μ-nitrido, and μ-carbido complexes were synthesized according to published protocols.[27]

Methods. The UV−visible (UV−vis) absorption spectra were recorded on an Agilent 8453 diode-array spectrophotometer. ^1H and ^{13}C NMR spectra were acquired on a Bruker Ascend 400 spectrometer. The reaction products were identified by NMR and GC-MS method (Hewlett-Packard 5973/6890 system; electron impact at 70 eV, He carrier gas, 30 m x 0.25 mm ROTICAP-5 capillary column, polyethylene glycol, 0.25 μm coating).

Mössbauer Experiments. The Mössbauer spectra were recorded on unenriched powders contained in Delrin cups at ca. 5 and 80 K on a strong-field Mössbauer spectrometer equipped with an Oxford Instruments Spectromag 4000 cryostat containing an 8 T split-pair superconducting magnet. The spectrometer was operated in a constant acceleration mode in transmission geometry. The isomer shifts were referenced against that of a room-temperature metallic iron foil. Analysis of the data was performed with the software WMOSS Mössbauer Spectral Analysis Software (http://www.wmoss.org), 2012−2013 (Web research, Edina).

Computational Details. Quantum chemistry calculations on model complexes without propyl substituents $(FePz)_2X$ were performed using DFT in the Kohn−Sham framework. Calculations on geometry optimizations and Mössbauer parameters were done using Amsterdam Density Functional (ADF) 2016[54−56] and Orca

DOI: 10.1021/acs.inorgchem.9b02718
Inorg. Chem. XXXX, XXX, XXX−XXX

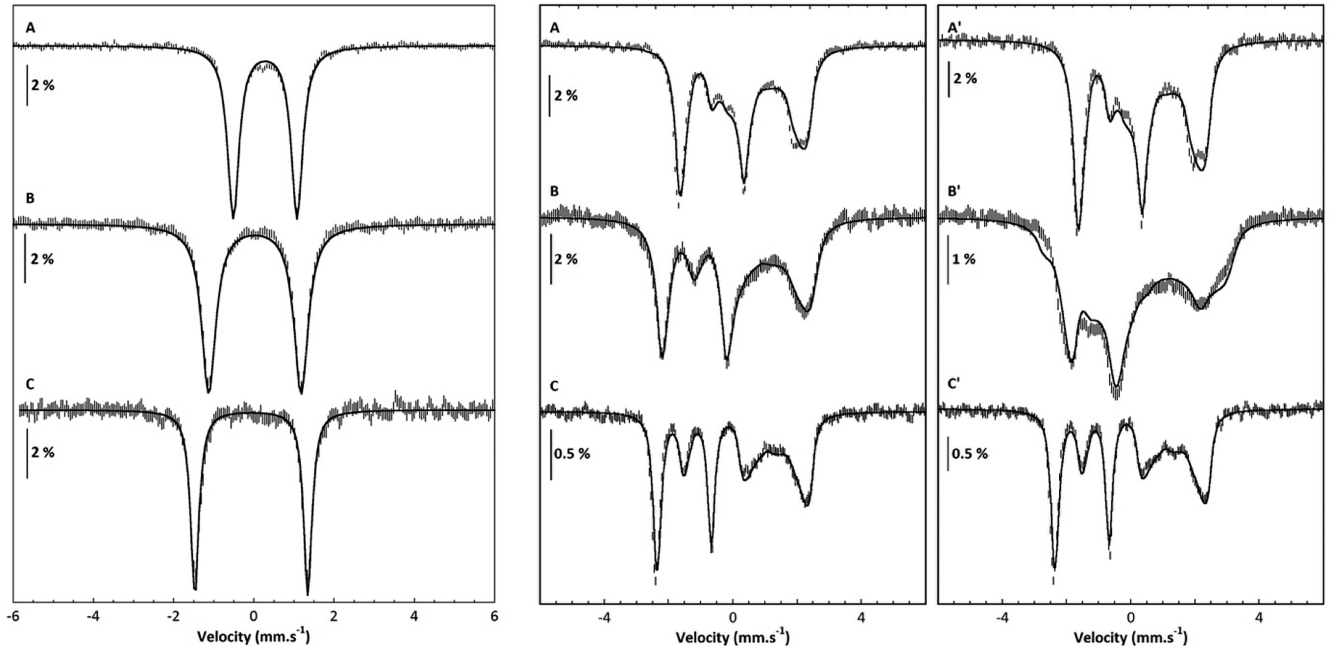

Figure 2. Mössbauer spectra of $(FePzPr_8)_2O$ (top), $(FePzPr_8)_2N$ (middle), and $(FePzPr_8)_2C$ (bottom) recorded (left panel) at 80 K under no magnetic field and (right panel) under a field of 7 T applied parallel to the γ rays at 80 K (A−C) and 5.5 K (A′−C′). Experimental spectra: hatched bars, black line: simulation using the parameters listed in Table 1.

3.0.1.[57−59] Some bonding analyses were performed with NBO 6.0[60,61] interfaced with ADF.

In ADF, geometry optimizations were carried out using the B3LYP[62] functional with Grimme D3[63] dispersion correction (B3LYP-D3 below) and the Slater triple-ζ + 2 polarization functions for all atoms (all-electron TZ2P set).[64] Mössbauer parameter calculations on the optimized geometries were performed according to published procedure.[65,66] Geometry optimizations with Orca were done with B3LYP and the D3BJ correction[67] using the Def2-tzvp basis sets[68,69] and the RIJCOSX approximation.[70,71]

Particular caution was taken to control local spin densities (see Supporting Information for details) at each stage (geometry optimizations and Mössbauer parameters). In particular, all calculations on singlet states were done in an unrestricted scheme. The electronic affinities (EA) of the carbene active species were calculated as the adiabatic difference of electronic energies between the complex and its one-electron reduced species using the same conditions as for above-mentioned geometry optimizations (ADF 2016 in gas phase with B3LYP-D3 and all-electron TZ2P sets) followed by single-points with COSMO[72] model solvent using acetonitrile (ε = 37).

Typical Procedure for Cyclopropanation of Olefins. All olefins were filtered through basic alumina and silica before use. A solution containing olefin (1 M) and $[FePzPr_8]_2X$ (1 mM) in 0.4 mL toluene was flushed with argon for 5 min. A 2 M solution of EDA in toluene (0.23 mL, 0.48 mmol, 1.2 equiv) was added to the reaction mixture under argon atmosphere via a syringe pump over 2, 4, or 6 h at 70 °C. The reaction mixture was magnetically stirred for 6 h. The reaction products were analyzed by ^{1}H NMR ($CDCl_3$) and by GC-MS. Analytical data for the reaction products were identical to those published in the literature.

Typical Procedure for Competitive Cyclopropanation of Olefins (Hammett Correlations). A 2 mM catalyst solution and a solution containing 1 M of styrene and 1 M of substituted styrene were prepared in toluene separately and were used for the preparation of the reaction mixture under argon. A 2 M solution of EDA in toluene (0.05 mL, 0.1 mmol, 0.25 equiv) was added over 1 h to a 0.4 mL solution containing 0.5 M styrene and 0.5 M *para*-substituted styrene, and 1 mM $(FePzPr_8)_2X$ in toluene was added by syringe pump under argon. The reaction mixture was magnetically stirred at 70 °C until EDA was consumed. The reaction products were analyzed by ^{1}H NMR ($CDCl_3$) and by GC-MS.

RESULTS AND DISCUSSION

Electronic Structures. μ-Oxo, μ-nitrido, and μ-carbido diiron complexes adopt Fe(III)(μ-O)Fe(III), Fe(III)(μ-N)Fe(IV), and Fe(IV)(μ-C)Fe(IV) oxidation states. Mössbauer spectra of these complexes have been recorded at 5.5 and 80 K in absence of magnetic field and under 2 and 7 T magnetic fields applied parallel to the γ rays. In absence of magnetic field (Figure 2, left panel), all spectra appear as a quadrupole doublet. In series $(FePzPr_8)_2O$, $(FePzPr_8)_2N$, $(FePzPr_8)_2C$, the center of the doublet (isomer shift) moves toward lower velocity, while the separation between the two lines (quadrupole splitting) increases (Table 1). Application of a strong magnetic field of 7 T at 80 or 5.5 K causes a splitting of these doublets into multiplets in the velocity range from −2.5 to 2.5 mm s^{-1} in all cases (Figure 2, right panel). This limited range is consistent with a low-spin nature of the compounds, S = 0 for μ-O and μ-C and S = 1/2 for μ-N complexes. For each compound, all three spectra could be simulated using this assumption with the parameters given in Table 1 (Figure 2).

The isomer shift and quadrupole splitting values of μ-O, μ-N, and μ-C bridged diiron tetraphenylporphyrin, phthalocyanine, and porphyrazine complexes are assembled in Table 1. A general decrease of the isomer shift is observed in the series $[(macrocycle)Fe]_2(\mu\text{-O})$, $[(macrocycle)Fe]_2(\mu\text{-N})$, $[(macrocycle)Fe]_2(\mu\text{-C})$ for all macrocycles in line with a progressive increase in the iron overall oxidation state. In parallel, a notable increase of the quadrupole splitting values occurs. A possible origin of this trend may be found in the increased covalency of the Fe−X bond due to the increase in its double bond character in the μ-O, μ-N, μ-C series.[25,27] Analysis of Mössbauer parameters in Table 1 shows that the electronic structure of the porphyrazine derivatives is closer to that of the corresponding phthalocyanine than that of the

DOI: 10.1021/acs.inorgchem.9b02718
Inorg. Chem. XXXX, XXX, XXX−XXX

Table 1. Isomer Shifts and Quadrupole Splittings of μ-Oxo, μ-Nitrido, and μ-Carbido Bridged Iron Macrocyclic Complexes

	T (K)	δ (mm s^{-1})	ΔE_Q (mm s^{-1})	ref
[(TPP)Fe]$_2$(μ-O)	131	0.40	0.62	73
[(Pc)Fe]$_2$(μ-O)	77	0.25	1.26	74
[(Pz)Ph$_8$)Fe]$_2$(μ-O)	297	0.40	0.89	75
[(PzPr$_8$)Fe]$_2$(μ-O)	77	0.23	1.31	this work
[(TPP)Fe]$_2$(μ-N)	131	0.18	1.08	73
[(TPP)Fe](μ-N)[(Pc)Fe]	77	0.11	1.47	76
[(Pc)Fe]$_2$(μ-N)	77	0.06	1.76	77
[(Pz)Ph$_8$)Fe]$_2$(μ-N)	298	−0.04	1.77	78
[(PzPr$_8$)Fe]$_2$(μ-N)[a]	77	0.03	1.91	this work
[(TPP)Fe]$_2$(μ-C)	77	0.10	1.89	79
[(Pc)Fe]$_2$(μ-C)	77	−0.03	2.69	79
[(PzPr$_8$)Fe]$_2$(μ-C)	77	−0.06	2.78	this work

[a]Spin Hamiltonian parameters g_x, g_y = 2.18, g_z = 2.0; A_x, A_y = −5.75 T, A_z = 6.47 T; η = 0.02.

tetraphenylporphyrin counterparts. In particular, for all [(macrocycle)Fe]$_2$(μ-X) compounds, δ_{PzPr8} is slightly inferior to δ_{Pc} which is 0.13(2) less than δ_{TPP}. Consistently, the electrochemical study of the related nitrido bridged complexes of alkyl-substituted macrocycles revealed the same trend for the oxidation of the [(macrocycle)Fe^{III}(μ-N)-Fe^{IV}(macrocycle)] core: $E_{1/2}{}^{PzPr8} < E_{1/2}{}^{Pc} \ll E_{1/2}{}^{TPP}$.

To get a deeper insight into the electronic structure of these complexes, we performed DFT calculations on (FePz)$_2$X model compounds containing no propyl groups. The Mössbauer data clearly pointed to low-spin systems, which are known to be a difficult case in the DFT framework owing to the multiconfigurational nature of a low-spin state wave function. Nevertheless, the broken symmetry (BS) approximation may give information on such electronic configuration. The monodeterminantal solution able to describe such low-spin wave function depends on the local Fe spin state and thus related to its individual S_z component. The possible BS solutions arising for X = O or C are shown in Table 2, together with their high-spin counterpart.

For X = N, the X-ray structure[27] and Mössbauer data point to a doublet spin state and to a strict equivalence of the two Fe ions. This observation implies that one unpaired electron is delocalized on both atoms. To explore these various electronic configurations, it was necessary to monitor strictly the guesses initiating the electronic convergence and to check the final local spin densities (see Supporting Information for details). The various possible BS solutions were thus calculated, and their energetic ordering is summarized in Table 2. In some cases, the BS solution could not be obtained. For instance, for X = C, the final wave function was always converging to local S_z = 0 whatever the initial guess. Some high-spin solutions are not shown in Table 2 (S = 5 for X = O, S = 3/2 for X = N, and S = 1 or 2 for X = C) because they converged to wave functions with nonequivalent Fe ions and were much higher in energies.

Table 2. Spin Configurations (BS for S = 0 and High Spin) Solutions for (FePz)$_2$X with X = O or C Depending on Individual Fe S_z, and Their Energetic Ordering (ΔE in kcal/mol)[a]

X	total S	BS solutions	ΔE
O	0	+1/2, −1/2	noCV
	0	+3/2, −3/2	0.0
	0	+5/2, −5/2	4.8
	3		25.8
C	0	0, 0	0.0
	0	+1, −1	noCV
	0	+2, −2	noCV
	2		64.8

[a]NoCV means that this BS solution could not be obtained.

Our exploration of various spin states for the three compounds led to the conclusion that the low-spin configuration was always by far the most stable one, that is, a singlet state for μ-O and μ-C and a doublet state for μ-N compounds. A good agreement was obtained between B3LYP with D3 correction optimized geometries and the experimentally resolved X-ray structures,[27] allowing for the calculation of Mössbauer parameters which were in good agreement with experimental data (Table 3).

Although the isomer shifts for (FePzPr$_8$)$_2$N and (FePzPr$_8$)$_2$C were less well reproduced, the general trend was in line with the experimental data, in particular, with the decrease in isomer shift from μ-O to μ-N and to μ-C complexes. The three complexes exhibit very different local spin densities rationalized according to their formal oxidation state. The (FePz)$_2$O complex contains two antiferromagnetically coupled Fe^{III} ions (J = −976 cm^{-1} calculated with the Yamaguchi formalism[80] using as spin Hamiltonian: $H = -2J \times S_A \times S_B$) with local quartet Fe spin configurations. For (FePz)$_2$N, our calculation shows a completely delocalized radical over the two equivalent Fe(+3.5) atoms consistently with our Mössbauer data and previous studies.[13,15,27,81] For (FePz)$_2$C with two Fe^{IV} sites, various broken symmetry configurations obtained by spin flipping from singlet, triplet, or quintet local Fe states always converged to local singlet Fe^{IV} ions. The Kohn−Sham orbital (MO) diagrams of these species allow us to give a unified picture of the three species depicted schematically in Figure 3. The resulting MOs can be analyzed in terms of symmetric (S) and antisymmetric (AS) combinations of Fe d AOs vs the plane perpendicular to the mean Fe−X−Fe axis defined as the z axis and going through the X position. The $d_{x^2-y^2}$ AOs are involved in σ bonds with N atoms from the Pz macrocycles, so their antibonding combinations are unoccupied and lie high in energy. The Fe−X−Fe bonding features are thus based on S and AS combinations of d_{z^2}, d_{xz}, and d_{yz} overlapping with symmetry-adapted 2s, 2p$_x$, 2p$_y$, and 2p$_z$ AOs of X to yield bonding/antibonding MOs (Figure S1). The AS combination of (d_{xz}, d_{yz}) orbitals is nonbonding as well as the d_{xy} orbitals (Figure S1). The resulting MO diagrams are shown in Figure 3 focusing only on the nonbonding or antibonding d centered orbitals, whereas the bonding contributions lie lower in energies and are not shown.

In all three complexes, the (d_{xz}, d_{yz})^S set forms two fully occupied π bonds involving 2p$_x$ and 2p$_y$ AOs of the bridging X atom, while their antibonding counterparts are unoccupied. These two π-bonds are delocalized on the Fe−X−Fe atoms, one π bond per Fe−X. A Fe−X−Fe σ^{AS} bond is formed from a $d_{z^2}{}^{AS}$ and 2p$_z$ (X) combination, occupied by two electrons, whereas its antibonding component is unfilled resulting in 0.5 σ^{AS} bond per Fe−X. The MO mostly concerned by the change in number of d electrons when going from μ-O to μ-C is the σ^{S}* orbital from $d_{z^2}{}^{S}$ combined to the 2s (X) orbital. This

DOI: 10.1021/acs.inorgchem.9b02718
Inorg. Chem. XXXX, XXX, XXX−XXX

Table 3. Calculated Data with B3LYP-D3 on $(FePz)_2X$ (X = O, N, C)[a]

	X = O		X = N		X = C	
structure	exp.	calcd	exp.	calcd	exp.	calcd
Fe−N(Pz)	1.955	1.95	1.93	1.945	1.915	1.94
Fe−X	1.777	1.77	1.655	1.64	1.67	1.64
Fe−X−Fe	158	155.9	168.6	160	175.1	179.8
h(Fe)	0.35	0.4	0.28	0.28	0.22	0.21
ρ						
Fe1		2.48		0.43		0
Fe2		−2.48		0.44		0
X		0.0		0.14		0
Mössbauer						
ΔE_Q	1.32	1.02	1.93	1.90	2.82	2.31
δ	0.23	0.29	0.03	0.22	−0.07	0.13

[a]main structural parameters (distances and height from the mean Pz plane h(Fe) in Å, angle Fe−X−Fe in deg) compared to X-ray data,[27] Mulliken spin densities (ρ), and Mössbauer parameters (mm s^{-1}). X = O and C: singlet state; X = N: doublet state.

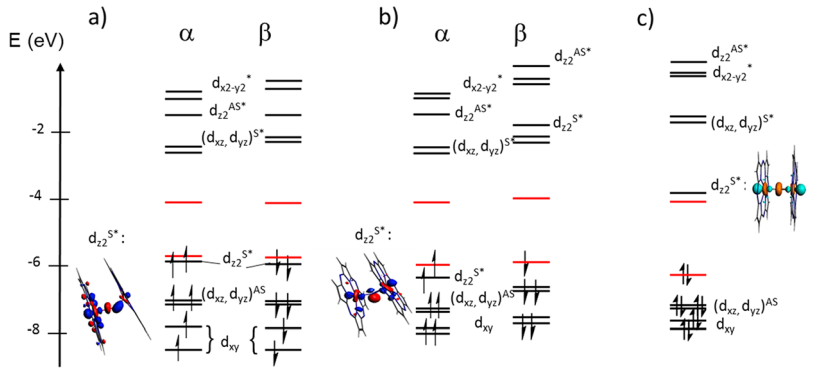

Fe-X bond	1 π, 0.5 σ	1 π, 0.75 σ	1 π, 1 σ
Fe-X Mayer b. o.	1.07	1.56	1.79

Figure 3. Schematic Kohn−Sham orbital diagrams of $(FePz)_2X$ species for (a) X = O (d^{10}); (b) X = N (d^9); (c) X = C (d^8). The valence configuration for μ-O, μ-N or μ-C is s^2p^6 in all cases (corresponding to formally "O^{2-}", "N^{3-}" or "C^{4-}" valencies). For the sake of simplicity, Fe−X bonding orbitals and orbitals localized on the macrocycles are not shown except for HOMO and LUMO (shown in red), which are made up of π and π^* orbitals from the Pz rings. Bottom: σ and π Fe−X bond composition as well as Mayer bond orders (b. o.).

Scheme 1. Cyclopropanation of Styrene by EDA Catalyzed by $(FePzPr_8)_2X$ (X = O, N, C)

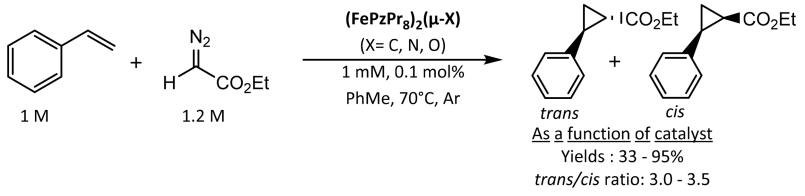

antibonding orbital contains two electrons for X = O (Figure 3a) leading to a net bond order of 0 for the Fe−O−Fe σ^S bond. In turn, for X = C the σ^{S*} orbital is unoccupied yielding a Fe−C−Fe σ^S bond order of 1. In case of X = N, the σ^{S*} orbital is the SOMO containing the unpaired electron equally delocalized over the two Fe d_{z^2} orbitals and the observed spin densities of ca. 0.5 on each Fe. Careful examination of this σ^{S*} orbital rationalizes the decrease in Fe−X−Fe bending angle from X = O to C (see Table 2). It is doubly occupied in $(FePz)_2O$, and the bending tends to release somewhat the energetic destabilization of this orbital, by favoring weak bonding overlaps between an O hybrid orbital (2s + 2p) and the in-plane ring of both d_{z^2} orbitals. This behavior is still present with a somewhat less extent for μ-N complex, as only one electron fills the antibonding σ^{S*} and is absent for μ-C species which is almost linear. The Mayer bond orders (Figure 3) illustrate the increase in Fe−X bond orders from $(FePz)_2O$ to $(FePz)_2C$. These electronic configurations are also in agreement with the evolution of quadrupole splitting values from μ-O to μ-C complex, pointing to an increase of the covalency and with the electronic equivalence of both Fe sites revealed in the Mössbauer study. This in-depth study confirms and completes the previous calculations that were published on single-atom bridged species.[25,27]

Evaluation of Catalytic Properties in Cyclopropanation of Styrene. The aforementioned difference in the electronic properties of the three dimeric complexes might result in the different catalytic behavior. Therefore the catalytic

DOI: 10.1021/acs.inorgchem.9b02718
Inorg. Chem. XXXX, XXX, XXX−XXX

activity of the three dimeric complexes was investigated in the cyclopropanation of styrene by ethyl diazoacetate (EDA) using 0.1 mol % catalyst loading (Scheme 1).

A 2 M EDA solution was added slowly to the solution of styrene and catalyst in toluene at 70 °C to favor cyclopropanation of styrene derivatives over EDA dimerization. Importantly, the high yield of cyclopropanation products can be achieved when styrene was the limiting reagent and 1.2 equiv EDA was used. It should be noted that in many studies, a large excess of olefin substrate has been used to limit the formation of undesirable EDA dimerization products which resulted in low cyclopropanation yields based on the initial substrate amounts.[30,33,35,37,48,50] Importantly, the comparison of the UV−vis spectra of $(FePzPr_8)_2O$, $(FePzPr_8)_2C$, and $(FePzPr_8)_2N$ recorded before and after catalytic reactions confirmed that all complexes retained their dimeric structures under catalysis conditions (Figures S2−S4). Thus, $(FePzPr_8)_2O$, $(FePzPr_8)_2C$, and $(FePzPr_8)_2N$ rather than their mononuclear $FePzPr_8$ counterpart are involved in the cyclopropanation reaction. When the reactions were carried out without styrene substrate, diethyl maleate and fumarate were formed, and the intensities of UV−vis spectra of all dimeric complexes were decreased indicating their partial degradation in the absence of substrate (Figures S5−S7). The time courses of the cyclopropanation of styrene in the presence of the three dimeric complexes clearly show superior activity of $(FePzPr_8)_2O$ (Figure 4).

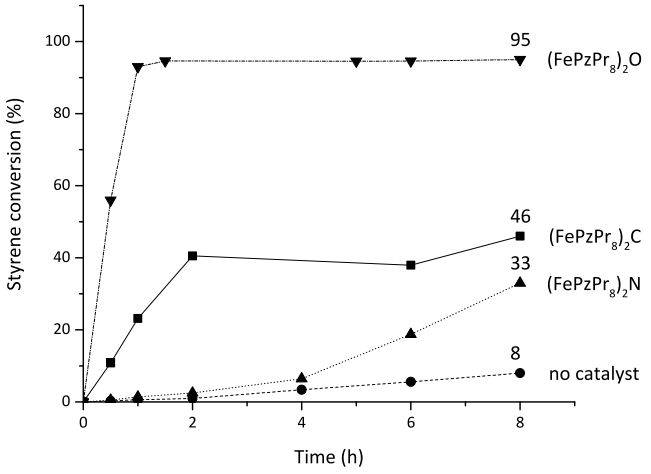

Figure 4. Time courses of the styrene cyclopropanation with EDA in the presence of $(FePzPr_8)_2O$, $(FePzPr_8)_2N$ and $(FePzPr_8)_2C$ at 70 °C.

The reaction between styrene and EDA at 70 °C without catalyst produced ∼1% and 8% yields of cyclopropanation products in a 64:36 *trans*/*cis* ratio after 1 and 6 h, respectively (Table 4).

In the presence of 0.1 mol % $(FePzPr_8)_2O$, a 95% yield of the cyclopropanation products was achieved at 70 °C after 1 h. The reaction was also efficient at 60 °C, although the product yield decreased to 73% accompanied by the increase of the amount of EDA dimerization products. The $(FePzPr_8)_2O$ complex did not react with EDA at 25 °C. The corresponding μ-carbido and μ-nitrido diiron complexes furnished lower yields of cyclopropanation products at 70 °C after 8 h: 46 and 33%, respectively. Interestingly, $(FePzPr_8)_2C$ was as efficient as $(FePzPr_8)_2O$ at 100 °C affording cyclopropanation products with a 97% yield after 1 h reaction. The $(FePzPr_8)_2N$ complex showed a lower catalytic activity. All three dimeric complexes exhibited similar moderate *trans*/*cis* ratios of cyclopropanation products. In the case of sterically unhindered porphyrin complexes, the high *trans*/*cis* ratios (>8) were associated with the involvement of the less-electrophilic Fe(II) carbene intermediates, while low *trans*/*cis* selectivity could be considered as an indication for more electrophilic Fe(III) species.[82] Thus, relatively low *trans*/*cis* selectivity of the cyclopropanation mediated by $(FePzPr_8)_2X$ complexes is compatible with their high oxidation states.

Several diazo carbene precursors were evaluated in combination with $(FePzPr_8)_2O$. Benzyl diazoacetate provided a 95% yield of cyclopropanation products with increased selectivity to *trans*-cyclopropyl derivative with *trans*/*cis* ratio of 84:16 (Table 4, entry 10). However, *t*-butyl diazoacetate was less suitable for cyclopropanation of styrene owing to the preferential formation maleate and fumarate derivatives (Table 4, entry 11). Trimethylsilyldiazomethane furnished 1-phenyl-2-trimethylsilylcyclopropanes with a 47% yield in 83:17 *trans*/*cis* ratio (Table 4, entry 12).

The scope of the reaction was extended using $(FePzPr_8)_2O$ catalyst under optimal conditions: 0.1 mol % catalyst loading, 1.2 M EDA, and 1 M amine in toluene at 70 °C for 2 h reaction time (Table 5).

Anilines bearing electron-donating or electron-withdrawing groups afforded cyclopropanation products with excellent to quantitative yields with similar *trans*/*cis* ratio accompanied by minor amounts of EDA dimerization products. Importantly, the presence of electron-withdrawing substituents was well tolerated. Even pentafluorostyrene was cyclopropanated with a 89% yield, and the dimerization of EDA was limited to 11% (Table 5, entry 6). Bulky 1,1-diphenylethylene was converted to corresponding cyclopropyl derivative with a quantitative yield (Table 5, entry 8). However, cyclohexene was unreactive, and a significant amount of diethyl maleate was formed (Table 5, entry 9). In contrast, *n*-butylvinylether furnished a good cyclopropanation yield. The presence of methyl substituent at double bond in α-methylstyrene did not prevent the reaction, and corresponding cyclopropane was obtained with quantitative yield (Table 5, entry 7). In turn, 2,3-dimethyl-1,3-butadiene afforded mono- and double cyclopropanation products with 66 and 33% yields, respectively (Table 5, entry 11).

Hammett Correlations. The influence of the electronic structure of styrene derivatives on the reactivity was investigated for the three $(FePzPr_8)_2X$ complexes. The relative cyclopropanation rates k_X/k_H were determined in competitive reactions using 0.5 M concentrations of the *para*-substituted styrene and styrene and 0.25 M EDA. The relative rates were calculated as the molar ratio of cyclopropanation products obtained from the *para*-substituted styrene to that derived from styrene (Figure 5).

Different σ polar effect parameters (σ_p^+, σ_p, σ_{mb})[83,84] were correlated with $\log(k_X/k_H)$. The better correlations for all the complexes were obtained with σ_p^+ parameter which is consistent with the development of the partial positive charge in the transition state stabilized by resonance effects. However, $(FePzPr_8)_2O$ and $(FePzPr_8)_2C$ showed a moderate linearity (R^2 = 0.86), and no clear trend in the cyclopropanation of electron-rich and electron-deficient olefins was observed for $(FePzPr_8)_2N$ (Figure S8). Next, we performed a double parameter correlation using an approach introduced by Jiang

DOI: 10.1021/acs.inorgchem.9b02718
Inorg. Chem. XXXX, XXX, XXX−XXX

Table 4. Catalytic Cyclopropanation of Styrene by EDA Catalyzed by $(FePzPr_8)_2O$, $(FePzPr_8)_2C$ and $(FePzPr_8)_2N$ Complexes

				cyclopropanation		
entry	catalyst	temperature (°C)	reaction time	yield[a] (%)	*trans*/*cis*	EDA dimerization yield[b] (%)
1	no catalyst	70	1 h (8 h)	<1 (8)	64:36	0
2	no catalyst	100	1 h (6 h)	3 (24)	64:36	1 (2)
3	$(FePzPr_8)_2O$	60	75 min	73	77:23	37
4	$(FePzPr_8)_2O$	70	1 h	95	77:23	8
5	$(FePzPr_8)_2O$	100	1 h	95	70:30	18
6	$(FePzPr_8)_2C$	70	8 h	46	78:22	36
7	$(FePzPr_8)_2C$	100	1 h	97	70:30	21
8	$(FePzPr_8)_2N$	70	8 h	33	75:25	38
9	$(FePzPr_8)_2N$	100	1 h (6 h)	30 (46)	64:36	1
			Benzyl Diazoacetate			
10	$(FePzPr_8)_2O$	70	2 h	95	84:16	8
			t-Butyl Diazoacetate			
11	$(FePzPr_8)_2O$	70	2 h	17	88:12	40
			Trimethylsilyldiazomethane			
12	$(FePzPr_8)_2O$	70	2 h	47	83:17	23

[a]Yields of cyclopropanation products are based on the initial amount of styrene. [b]Yields of EDA dimerization products are based on the initial amount of EDA.

Table 5. Catalytic Cyclopropanation of Aromatic and Aliphatic Olefins by EDA Catalyzed by $(FePzPr_8)_2O$

		cyclopropanation		
entry	substrate	yield[a] (%)	*trans*/*cis* ratio	EDA dimerization, yield of *cis*/*trans*[b] (%)
1	4-methoxystyrene	100	76:24	6/0
2	4-methylstyrene	100	77:23	6/0
3	3-methylstyrene	99	76:24	8/<1
4	4-fluorostyrene	82	73:27	17/1
5	4-cyanostyrene	100	68:32	9/<1
6	pentafluorostyrene	89	80:20	11/1
7	α−methylstyrene	100	63:37	7/<1
8	1,1-diphenylethylene	100	–	5/<1
9	cyclohexene	0	–	76/3
10	*n*-butylvinylether	58	55:45	19/1
11	2,3-dimethyl-1,3-butadiene[c]	66	71:29	12/<1

[a]Yields of cyclopropanation products are based on the initial amount of olefin. [b]Yields of EDA dimerization products are based on the initial amount of EDA. [c]Yield of the products of double cyclopropanation was 33%.

to take into account spin-delocalization effect occurring when radical species are involved.[84] Double parameter linear regressions were carried out to evaluate the relative impact of both polar effect and spin delocalization using different σ polar effect parameters (σ_p^+, σ_p, σ_{mb}) in combination with the $\sigma_{JJ}^\bullet$ spin delocalization parameter. Although a better correlation was obtained with $\sigma_{JJ}^\bullet/\sigma_p^+$ pair, no notable improvement in linearity was obtained compared with classical Hammett correlations (R^2 = 0.86, 0.57, and 0.87 for μ-O, μ-N, and μ-C complexes, respectively) (Figure S9).

The observed nonlinearity might be indicative of intermediates that have significant radical character.[85] Notable improvement of correlation was obtained when Creary's radical $\sigma_c^\bullet$ parameters were used. These parameters were determined in the thermal rearrangement of 1,1-dimethyl-2-methylenecyclopropanes in C_6D_6 at 80 °C (set A)[86] and in isooctane at 100 °C (Set B).[87] Using set B parameters, significantly better linearity was achieved for $(FePzPr_8)_2C$ (R^2 = 0.99) and $(FePzPr_8)_2O$ (R^2 = 0.97) whereas the correlation obtained for $(FePz)_2N$ (R^2 = 0.86) was still moderate (Figure 6).

Noteworthy, in the case of $(FePzPr_8)_2N$, the k_X/k_H values are not very sensitive to the electronic nature of *para*-substituent of styrene excepting *p*-methoxystyrene in all attempted correlations (Figures 6, S8, and S9). This finding suggests that in this case, the rate-limiting step might be the formation of $(FePzPr_8)_2N$-carbene species rather than its reaction with styrene derivative. μ-Nitrido complex with Fe(III)Fe(IV) site is probably not sufficiently nucleophilic to assist N_2 release from the complexed EDA to generate carbene species. The similar reactivity of $(FePzPr_8)_2N$ at 70 and 100 °C (Table 4, entries 7 and 8) is in accordance with this suggestion. The increased activity of *p*-methoxystyrene can be

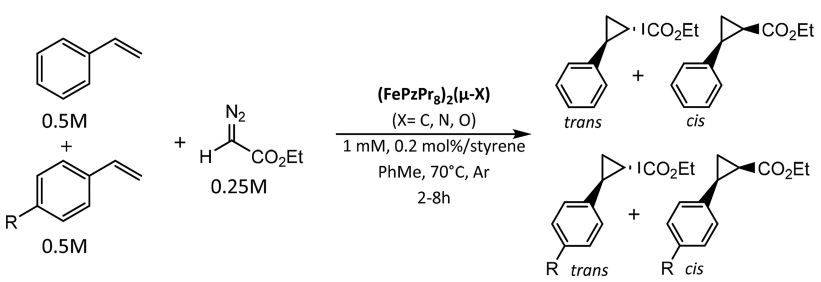

Figure 5. Determination of the relative rates of the cyclopropanation of *para*-substituted styrene with respect to styrene.

DOI: 10.1021/acs.inorgchem.9b02718
Inorg. Chem. XXXX, XXX, XXX−XXX

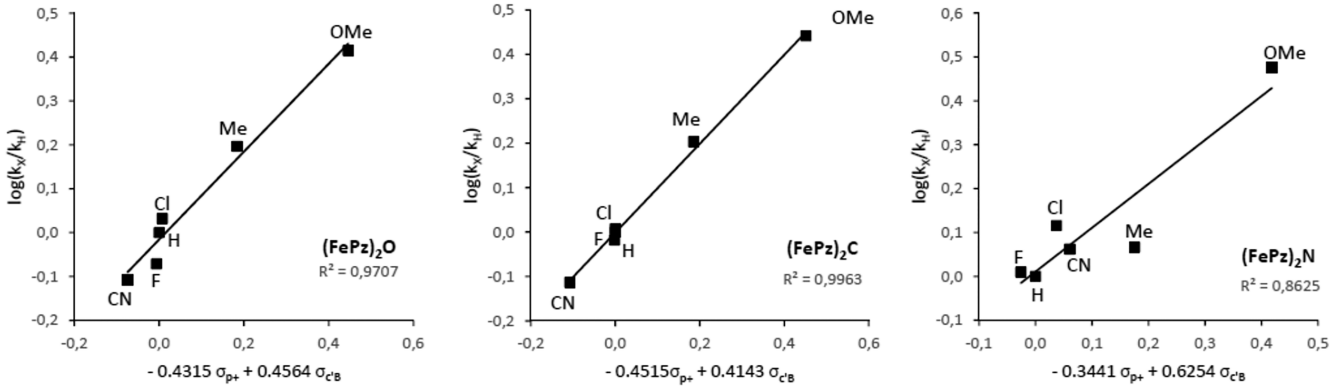

Figure 6. Correlation plots of $\log(k_X/k_H)$ vs $(\rho_{JJ}^{\bullet}\,\sigma_c^{\bullet} + \rho_p^{+}\,\sigma_p^{+})$ for the cyclopropanation of *p*-Y-substituted styrenes by ethyl diazoacetate catalyzed by $(FePzPr_8)_2X$.

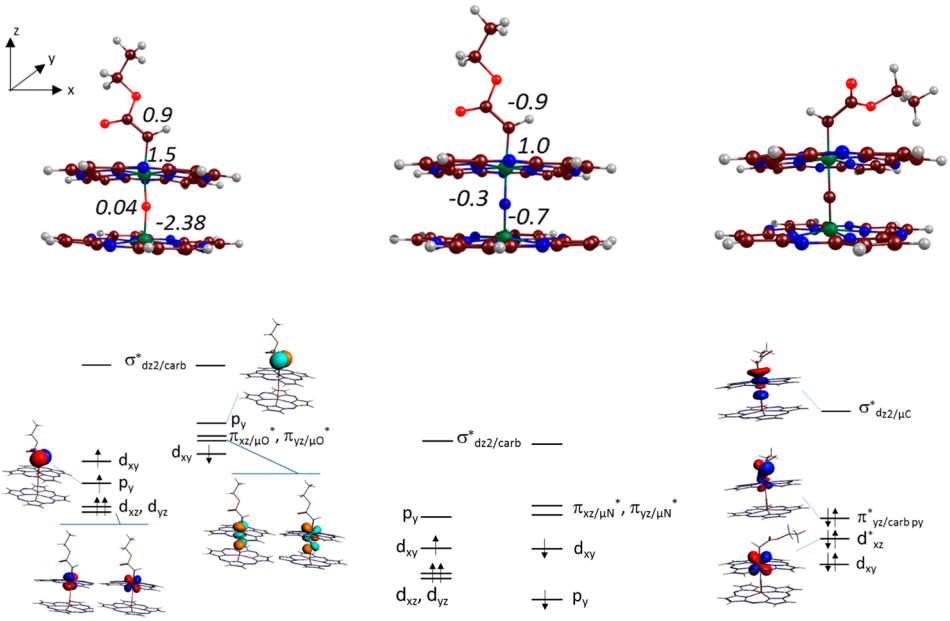

Figure 7. Top panel: Structures of carbene $(FePz)_2X$-based complexes (left: X = O, middle: X = N, right: X = C) optimized with B3LYP-D3 and NPA spin densities at iron, carbene, and bridging atoms (not shown for closed-shell μ-C complex). Bottom panel: NBO analysis showing only the proximal iron d-antibonding orbitals and p_y AO of the carbene involved in its radical character. Key orbitals are displayed for μ-O and μ-C complexes and not shown for μ-N complex for the sake of simplicity because they are very similar to those of μ-O complex.

explained by its nucleophilic properties strong enough to attack directly the $(FePzPr_8)_2N$-EDA intermediate before N_2 release according to the mechanism proposed by Gross for nitrogen- and sulfur-containing nucleophilic compounds.[88] The negative values of ρ_p^{+} (−0.43, −0.45, and −0.34 for μ-O, μ-C, and μ-N complexes, respectively) are consistent with a nucleophilic attack of olefin on the iron carbene intermediate. Excellent Creary's correlations obtained with $(FePzPr_8)_2O$ and $(FePzPr_8)_2C$ suggest radical stepwise mechanism of the cyclopropanation reaction. The negative ρ_p^{+} values for all three complexes are comparable to those determined for this reaction mediated by iron porphyrin complexes,[40] indicating their electrophilic nature and the development of the positive charge at the olefin carbon atoms in the transition state. The $\rho_p^{+}/\rho_{C'}$ ratios of 0.95 and 1.09 obtained for μ-O and μ-C species, respectively, suggest that both polar and spin effects are important.[85]

Electronic Structure of Putative Carbene Complexes: Relationship with Reactivity. Several experimental and theoretical studies published on the olefin cyclopropanation mediated by EDA and mononuclear iron porphyrin-like catalysts point to an active intermediate having carbene axially bonded to the Fe site.[33,36,82,89−91] The observed catalytic activity of the three diiron complexes suggests that related carbene intermediates can be formed at binuclear platforms. We performed theoretical modeling on the putative $(FePz)_2X$-carbene species using the same DFT approach successfully used for the initial $(FePz)_2X$ species. The Fe site bearing the carbene group is noted Fe^p (proximal Fe) and another Fe site is noted Fe^d (distal Fe). Starting from the low-spin configuration of the $(FePz)_2X$ complex, the carbene brings two valence electrons which can be involved into bonds with the proximal Fe site. Thus, the resulting spin states of the carbenic species are expected to be open-shell singlet or triplet for $(FePz)_2O$ and $(FePz)_2C$ and doublet or quartet for

DOI: 10.1021/acs.inorgchem.9b02718
Inorg. Chem. XXXX, XXX, XXX−XXX

$(FePz)_2N$. Indeed, thorough exploration of the various spin states using broken-symmetry approaches showed that the ground state at the B3LYP level is a singlet for $(FePz)_2O$ and $(FePz)_2C$ and doublet for $(FePz)_2N$ carbene species. The main structural parameters and spin densities are shown in Table S4, and their structure is shown in Figure 7.

As expected, both Fe−X bonds of binuclear carbene complexes are not equivalent due to the axial bonding of the carbene group to Fe^P site. Mulliken as well as NPA spin densities clearly point to a radical character of the carbene in μ-O and μ-N species (see Table S4).

The bonding features were examined through a NBO analysis, and the most significant ones are described here, whereas detailed analyses of the localized orbitals are given in Supporting Information (Tables S5−S7). In the carbene $(FePz)_2O$ complex, the Fe^d site is an Fe^{III} ion in the intermediate spin local configuration. The Fe^P site in S = 1 Fe^{IV} local configuration has one σ bond with the carbene group and 2 π bonds with the bridging oxygen only for β orbitals. This σ bond between Fe^P and carbene is made up of the combination of the d_{z^2} and a hybridized sp_2 orbital of the carbene group with one electron provided by Fe^P and one by the carbene. The second carbenic valence electron remains as unpaired electron localized in a p_y AO. The bonding of Fe^P in the μ-N complex is very similar to that in μ-O species with a more covalent Fe^P-μN bond compared to Fe^P-μO as attested by the Wiberg bond orders (Table S8) and relative contributions of Fe^P and O/N orbitals (Tables S5 and S6). Both Fe sites in $(FePz)_2N$ are Fe^{IV} in local intermediate spin configurations.

The NPA population in the μ-carbido counterpart shows low-spin proximal Fe^{II} and distal Fe^{IV} sites. This Fe^P configuration is due to charge transfers from both μ-carbido and carbene carbon atoms through strong covalent bonds (Table S7). Indeed, the NPA charges (Table S9) are negative for μ-X and carbene group in μ-O and μ-N species, whereas they are both positive in the μ-C analogue, indicating esssential electron transfer to Fe^P. The carbene group in $(FePz)_2C$ is bonded to Fe^P by one π dative bond formed by combination of Fe^P d_{yz} and carbene $2p_y$ orbitals and occupied by two electrons provided by carbene group. The Wiberg bond orders (Table S8) reflect all these bonding features and are consistent with the trends in Fe−X and Fe−C (carbene) optimized distances.

Previous theoretical studies have been done on carbenic species issued from mononuclear Fe^{II} porphyrins,[89,92−94] while only a few studies on Fe^{III} porphyrin carbene species have been described.[36,95] Interestingly, we observe a similar behavior as that of Fe^{II} porphyrin carbene species described by Sharon et al.[93] In $(FePz)_2O$ and $(FePz)_2N$ species, the unpaired electron of carbene is localized on a p_y orbital which exhibits some delocalization onto the O atoms of the ester group yielding a planar structure of both Fe−C(H)COO moieties. For the closed-shell $(FePz)_2C$ species, the two electrons from the carbene are localized in a π bond formed with d_{yz}, and there is no more delocalization at the ester group. The resulting carbene structure is thus bent to the Pz ring, which is quite similar to what Sharon et al. observed for the mononuclear closed-shell singlet structure.[93]

The experimental reactivity data clearly point to a nucleophilic attack of the olefin double bond to carbene complex. We examined the frontier orbitals of these three complexes with a special focus on the LUMO. A slight increase in the LUMO eigenvalue from $(FePz)_2O$ to $(FePz)_2N$ and $(FePz)_2C$ species could be observed (Figure 8).

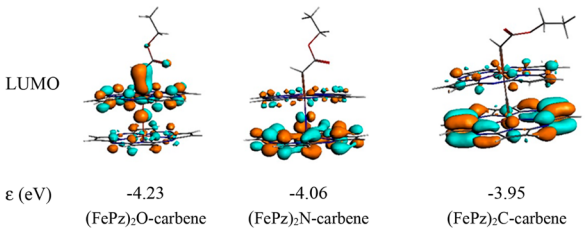

Figure 8. LUMO of the three $(FePz)_2X$-carbene species calculated with B3LYP/TZ2P, eigenvalues in eV.

The LUMOs for the $(FePz)_2N$ and $(FePz)_2C$ carbene complexes are localized on π^* orbitals of the distal Pz ligand that can explain their lower reactivity in the reaction with styrene. In the case of $(FePz)_2O$, LUMO is the unoccupied β $2p_y$ of the radical carbene species, which should be more favorable for the initial radical addition to double bond of styrene. The electron affinity of these three carbene species reveals a monotonic decrease: 101.1 kcal/mol for $(FePz)_2O$, 91.1 kcal/mol for $(FePz)_2N$, and 82.9 kcal/mol for $(FePz)_2C$. This is consistent with the trend in eigenvalues of the LUMO. This appears to be counterintuitive because the formal redox states of Fe ions in these complexes increase from μ-oxo to μ-carbido species. However, it should be taken into account that the whole molecules stay neutral and the bridging ligand becomes more and more donating from μ-oxo to the μ-nitrido and to the μ-carbido bridge. Recently, Wang et al. reported that electron-withdrawing substituents of quinoid carbene complex of Ru porphyrin lowered its electrophilicity in carbene transfer reaction.[96]

SUMMARY AND CONCLUSIONS

In this study, we have demonstrated for the first time that single-atom bridged diiron tetrapyrrolic complexes are capable of catalyzing the carbene transfer to styrenes affording cyclopropane derivatives. The order of the catalytic activity is Fe^{III}−O−Fe^{III} ≫ Fe^{IV}=C=Fe^{IV} > Fe^{III}−N=Fe^{IV}. The μ-oxo diiron complex showed excellent catalytic efficiency providing a 95% yield of cyclopropanation products based on substrate in 77:23 *trans*/*cis* ratio with 0.1 mol % catalyst loading (TON = 950). The reaction scope was successfully extended to aromatic olefins bearing either electron-donating or electron-withdrawing substituents and to aliphatic olefins. Other carbene precursors such as benzyl diazoacetate, trimethylsilyldiazomethane, and *t*-butyl diazoacetate can also be used, though the latter with less efficiency. The carbene transfer reactivity is usually associated with the involvement of metal carbene species.[30,40] Several mononuclear iron carbene complexes have been described though their electronic structure and is still a matter of debate in the literature.[89−94] To get insight into the possible involvement of putative carbene species on binuclear diiron platform, we have first performed a detailed DFT study of the three diiron porpyrazine complexes differing in the nature of bridging atom (μ-O, μ-N and μ-C) and in the iron oxidation state, $Fe^{III}\mu OFe^{III}$, $Fe^{III}\mu NFe^{IV}$, and $Fe^{IV}\mu CFe^{IV}$, respectively (Figure 1). DFT calculations provided useful information on the electronic properties of these complexes. The DFT-optimized structures of $(FePzPr_8)_2X$ (X = O, N, C) are consistent with

DOI: 10.1021/acs.inorgchem.9b02718
Inorg. Chem. XXXX, XXX, XXX−XXX

their crystal structures with discrepancies in bond distances <0.03 Å (Table 3). The simulated Mössbauer spectra compare well with the experimental data. Detailed analysis of Mössbauer data of diiron complexes involving different bridging atom and macrocyclic ligands clearly indicates that the electronic structure of the porphyrazine complexes is closer to that of the phthalocyanine rather than porphyrin analogs.

This approach validated in simulation of the three starting diiron complexes was successfully applied to gain insight into electronic structures of corresponding putative carbene species and to understand the influence of the electronic structure on reactivity. μ-O and μ-N carbene complexes bear significant spin density at the carbon carbene atom (0.9 e spin density) and thus can be described as radicaloid species. In contrast to $(FePz)_2N$ and $(FePz)_2C$ carbene complexes having LUMOs localized on π^* orbitals of the distal Pz ligand, LUMO of the μ-O counterpart is the unoccupied β $2p_y$ orbital of the radical carbon atom of carbene species. This difference in electronic structures can explain the lower reactivity of μ-C and μ-N species and much higher reactivity of μ-O species. Indeed, the latter structure should facilitate the initial radical addition to the double bond of styrene, followed by cyclization to form the cyclopropane ring. Further calculations on the reaction profiles involving activation of EDA upon coordination via nitrogen or carbon atoms of EDA and reaction with olefin are in progress.

In conclusion, among $(FePzPr_8)_2X$ complexes, μ-oxo diiron species exhibit a high reactivity in the cyclopropanation of olefins, adding another promising case to the wide range of catalytic applications of μ-oxo dimers.[97] Recent DFT studies indicate that carbene species on iron mononuclear porphyrinoid platforms can adapt several electronic configurations which might lead to their different reactivities.[98−100] In this context, binuclear counterparts can provide a large variety of the structural and electronic configurations and novel reactivity patterns and reaction landscapes can be disclosed.

■ ASSOCIATED CONTENT

Supporting Information

The Supporting Information is available free of charge at https://pubs.acs.org/doi/10.1021/acs.inorgchem.9b02718.

Experimental and additional computational details, correlation data on reactivity, Cartesian coordinates of computed structures (PDF)

■ AUTHOR INFORMATION

Corresponding Authors

*E-mail: pascale.maldivi@cea.fr.
*E-mail: jean-marc.latour@cea.fr.
*E-mail: alexander.sorokin@ircelyon.univ-lyon1.fr.

ORCID

Alexander B. Sorokin: 0000-0002-2699-6665

Notes

The authors declare no competing financial interest.

■ ACKNOWLEDGMENTS

Research support was provided by the Agence Nationale de Recherche (ANR, France, grant ANR-16-CE29-0018-01). L.P.C. is indepted to Ministère de l'Education Nationale, de l'Enseignement Supérieur et de la Recherche, France for his Ph.D. fellowship. This work was performed using HPC resources from GENCI-CINES and IDRIS (grants A0020807648 and A0040807648). P.M. and J.-M.L. thank Labex ARCANE and CBH-EUR-GS (ANR-17-EURE-0003) for partial support of this work.

■ REFERENCES

(1) Groves, J. T. Models and mechanisms of cytochrome P450 action. In *Cytochrome P450: structure, mechanisms, and biochemistry*, 3rd ed.; Ortiz de Montellano, P. R., Ed.; Kluwer Academic/Plenum Publishers: New York, 2005; pp 1−42.

(2) Costas, M. Selective C-H oxidation catalyzed by metalloporphyrins. *Coord. Chem. Rev.* **2011**, *255*, 2912−2932.

(3) Olivo, G.; Cussó, O.; Borrell, M.; Costas, M. Oxidation of alkane and alkene moieties with biologically inspired nonheme iron catalysts and hydrogen peroxide: from free radicals to stereoselective transformations. *JBIC, J. Biol. Inorg. Chem.* **2017**, *22*, 425−452.

(4) Bryliakov, K. P.; Talsi, E. P. Active sites and mechanisms of bioinspired oxidation with H_2O_2, catalyzed by non-heme Fe and related Mn complexes. *Coord. Chem. Rev.* **2014**, *276*, 73−96.

(5) Friedle, S.; Reisner, E.; Lippard, S. J. Current challenges of modelling diiron enzyme active sites for dioxygen activation by biomimetic synthetic complexes. *Chem. Soc. Rev.* **2010**, *39*, 2768−2779.

(6) Gouré, E.; Senthilnathan, D.; Coin, G.; Albrieux, F.; Avenier, F.; Dubourdeaux, P.; Lebrun, C.; Maldivi, P.; Latour, J.-M. Redox self-adaptation of a nitrene transfer catalyst to the substrate needs. *Angew. Chem., Int. Ed.* **2017**, *56*, 4305−4309.

(7) Gouré, E.; Avenier, F.; Dubourdeaux, P.; Sénèque, O.; Albrieux, F.; Lebrun, C.; Clémancey, M.; Maldivi, P.; Latour, J.-M. A diiron(III,IV) imido species very active in nitrene-transfer reactions. *Angew. Chem., Int. Ed.* **2014**, *53*, 1580−1584.

(8) Floris, B.; Donzello, M. P.; Ercolani, C. Single-Atom Bridged Dinuclear Metal Complexes with Emphasis on Phthalocyanine System. In *The Porphyrin Handbook*; Kadish, K. M., Smith, K. M., Guilard, R., Eds.; Academic Press: Amsterdam, 2003, Vol. *18*, pp 1−62.

(9) Pergrale, C.; Sorokin, A. B. Designing a dimeric phthalocyanine-supported catalyst for the selective oxidation of aromatic compounds. *C. R. Acad. Sci., Ser. IIc: Chim.* **2000**, *3*, 803−810.

(10) Zalomaeva, O. V.; Ivanchikova, I. D.; Kholdeeva, P. A.; Sorokin, A. B. Kinetics and mechanism of the oxidation of alkyl substituted phenols and naphthols with tBuOOH in the presence of supported iron phthalocyanine. *New J. Chem.* **2009**, *33*, 1031−1037.

(11) Afanasiev, P.; Sorokin, A. B. μ-Nitrido diiron macrocyclic platform: particular structure for particular catalysis. *Acc. Chem. Res.* **2016**, *49*, 583−593.

(12) Sorokin, A. B. μ-Nitrido diiron phthalocyanine and porphyrin complexes: unusual structures with interesting catalytic properties. *Adv. Inorg. Chem.* **2017**, *70*, 107−165.

(13) İşci, Ü.; Faponle, A. S.; Afanasiev, P.; Albrieux, F.; Briois, V.; Ahsen, V.; Dumoulin, F.; Sorokin, A. B.; de Visser, S. P. Site-selective formation of an iron(IV)-oxo species at the more electron-rich iron atom of heteroleptic μ-nitrido diiron phthalocyanines. *Chem. Sci.* **2015**, *6*, 5063−5075.

(14) Kudrik, E. V.; Afanasiev, P.; Alvarez, L. X.; Dubourdeaux, P.; Clemancey, M.; Latour, J.-M.; Blondin, G.; Bouchu, D.; Albrieux, F.; Nefedov, S. E.; Sorokin, A. B. An N-bridged high-valent diiron-oxo species on a porphyrin platform that can oxidize methane. *Nat. Chem.* **2012**, *4*, 1024−1029.

(15) Quesne, M. G.; Senthilnathan, D.; Singh, D.; Kumar, D.; Maldivi, P.; Sorokin, A. B.; de Visser, S. P. Origin of the enchanced reactivity of μ-nitrido-bridged diiron(IV)-oxo porphyrinoid complexes over cythochrome P450 compound I. *ACS Catal.* **2016**, *6*, 2230−2243.

(16) Alvarez, L. X.; Sorokin, A. B. Mild oxidation of ethane to acetic acid by H_2O_2 catalyzed by supported μ-nitrido diiron phthalocyanines. *J. Organomet. Chem.* **2015**, *793*, 139−144.

(17) Mihara, N.; Yamada, Y.; Takaya, H.; Kitagawa, Y.; Igawa, K.; Tomooka, K.; Fujii, H.; Tanaka, K. Site-selective supramolecular

DOI: 10.1021/acs.inorgchem.9b02718
Inorg. Chem. XXXX, XXX, XXX−XXX

complexation activates catalytic ethane oxidation by nitride-bridged iron porphyrinoid dimer. *Chem. - Eur. J.* **2018**, *25*, 3369−3375.
(18) Kudrik, E. V.; Sorokin, A. B. Oxidation of aliphatic and aromatic C-H bonds by t-BuOOH catalyzed by μ-nitrido diiron phthalocyanine. *J. Mol. Catal. A: Chem.* **2017**, *426*, 499−505.
(19) Seo, K.; Kim, H.; Lee, J.; Kim, M.-G.; Seo, S. Y.; Kim, C. Cooperative behavior of perfluoro carboxylic acid on cyclohexane oxidation catalyzed by μ-nitrido diiron phthalocyanine complex. *J. Ind. Eng. Chem.* **2017**, *53*, 371−374.
(20) Isci, U.; Afanasiev, P.; Millet, J.-M. M.; Kudrik, E. V.; Ahsen, V.; Sorokin, A. B. Preparation and characterization of μ-nitrido diiron phthalocyanines with electron-withdrawing substitients: application for catalytic aromatic oxidation. *Dalton Trans.* **2009**, 7410−7420.
(21) Alvarez, L. X.; Kudrik, E. V.; Sorokin, A. B. Novel reactivity of N-bridged diiron phthalocyanine in the activation of C-H bonds: hydroacylation of olefins as an example of the efficient C-C bond formation. *Chem. - Eur. J.* **2011**, *17*, 9298−9301.
(22) Colomban, C.; Kudrik, E. V.; Afanasiev, P.; Sorokin, A. B. Catalytic defluorination of perfluorinated aromatics under oxidative conditions using N-bridged diiron phthalocyanine. *J. Am. Chem. Soc.* **2014**, *136*, 11321−11330.
(23) Colomban, C.; Kudrik, E. V.; Afanasiev, P.; Sorokin, A. B. Degradation of chlorinated phenols in water in the presence of H_2O_2 and water-soluble μ-nitrido diiron phthalocyanine. *Catal. Today* **2014**, *235*, 14−19.
(24) Kroitor, A. P.; Cailler, L.; Martynov, A. G.; Gorbunova, Yu. G.; Tsivadze, A. Yu.; Sorokin, A. B. Unexpected formation of μ-carbido diruthenium(IV) complex during metallation of phthalocyanine with $Ru_3(CO)_{10}$ and its catalytic activity in the carbene transfer reactions. *Dalton Trans.* **2017**, *46*, 15651−15655.
(25) Colomban, C.; Kudrik, E. V.; Briois, V.; Shwarbrick, J. C.; Sorokin, A. B.; Afanasiev, P. X-ray absorption and emission spectroscopies of X-bridged diiron phthalocyanine complexes $(FePc)_2X$ (X = C, N, O) combined with DFT study of $(FePc)_2X$ and their high-valent diiron oxo complexes. *Inorg. Chem.* **2014**, *53*, 11517−11530.
(26) Bakshi, E. N.; Delfs, C. D.; Murray, M. S.; Peters, B.; Homborg, H. Iron(IV) phthalocyanines. Mössbauer spectral studies of (μ-carbido)(phthalocyaninato)iron(IV) and of its axially ligated and oxidized (Pc^{+} π cation radical) derivatives. *Inorg. Chem.* **1988**, *27*, 4318−4320.
(27) Colomban, C.; Kudrik, E. V.; Tyurin, D. V.; Albrieux, F.; Nefedov, S. E.; Afanasiev, P.; Sorokin, A. B. Synthesis and characterization of μ-nitrido, μ-carbido and μ-oxo dimers of iron octapropylporphyrazine. *Dalton Trans.* **2015**, *44*, 2240−2251.
(28) (a) Rodriguez-Morgade, M. S.; Stuzhin, P. A. The chemistry of porphyrazines: an overview. *J. Porphyrins Phthalocyanines* **2004**, *8*, 1129−1165. (b) Stuzhin, P. A. Iron complexes of octaphenyltetraazaporphine. *Makrogeterotsikly* **2009**, *2*, 114−129.
(29) Yusubov, M. S.; Celik, C.; Geraskina, M. R.; Yoshimura, A.; Zhdankin, V. V.; Nemykin, V. N. Binuclear iron(III) octakis-(perfluorophenyl)tetraazaporphyrin μ-oxodimer: a highly efficient catalyst for biomimetic oxygenation reactions. *Tetrahedron Lett.* **2014**, *55*, 5687−5690.
(30) Intrieri, D.; Carminati, D. M.; Gallo, E. Recent advances in metal porphyrinoid-catalyzed nitrene and carbene transfer reactions. In *Handbook of Porphyrin Science*; Kadish, K. M., Smith, K. M., Guilard, R., Eds.; World Scientific: Singapore, 2016; Vol. *38*, pp 1−99.
(31) Che, C.-M.; Huang, J.-S. Ruthenium and osmium porphyrin carbene complexes: synthesis, structure, and connection to the metal-mediated cyclopropanation of alkenes. *Coord. Chem. Rev.* **2002**, *231*, 151−164.
(32) Goswami, M.; de Bruin, B.; Dzik, W. I. Difluorocarbene transfer from a cobalt complex to an electron-deficient alkene. *Chem. Commun.* **2017**, *53*, 4382−4385.
(33) Wolf, R. J.; Hamaker, C. G.; Djukic, J.-P.; Kodadek, T.; Woo, L. K. Shape and stereoselective cyclopropanation of alkenes catalyzed by iron porphyrins. *J. Am. Chem. Soc.* **1995**, *117*, 9194−9199.
(34) Xu, X.; Wang, Y.; Cui, X.; Wojtas, L.; Zhang, X. P. Metalloradical activation of α-formyldiazoacetates for the catalytic asymmetric radical cyclopropanation of alkenes. *Chem. Sci.* **2017**, *8*, 4347−4351.
(35) Wang, Y.; Wen, X.; Cui, X.; Wojtas, L.; Zhang, X. P. Asymmetric radical cyclopropanation of alkenes with in situ-generated donor-substituted diazoreagents via Co(II)-based metalloradical catalysis. *J. Am. Chem. Soc.* **2017**, *139*, 1049−1052.
(36) Carminati, D. M.; Intrieri, D.; Caselli, A.; Le Gac, S.; Boitrel, B.; Toma, L.; Legnani, L.; Gallo, E. Designing 'totem' C_2-symmetrical iron porphyrin catalysts for stereoselective cyclopropanation. *Chem. - Eur. J.* **2016**, *22*, 13599−13612.
(37) Nicolas, I.; Le Maux, P.; Simonneaux, G. Synthesis of chiral water-soluble metalloporphyrins (Fe,Ru,): new catalysts for asymmetric carbene transfer in water. *Tetrahedron Lett.* **2008**, *49*, 5793−5795.
(38) Intrieri, D.; Carminati, M. D.; Gallo, E. The ligand influence in stereoselective carbene transfer reactions promoted by chiral metal porphyrin catalysts. *Dalton Trans.* **2016**, *45*, 15746−15761.
(39) Simonneaux, G.; Le Maux, P.; Ferrand, Y.; Rault-Berthelot, J. Asymmetric heterogeneous catalysis by metalloporphyrins. *Coord. Chem. Rev.* **2006**, *250*, 2212−2221.
(40) Li, Y.; Huang, J.-S.; Zhou, Z.-Y.; Che, C.-M.; You, X.-Z. Remarkably stable iron porphyrins bearing nonheteroatom-stabilized carbene or (alkoxycarbonyl)carbenes: isolation, X-ray crystal structure, and carbon atom transfer reactions with hydrocarbons. *J. Am. Chem. Soc.* **2002**, *124*, 13185−13193.
(41) Gross, Z.; Galili, N.; Simkhovich, L. Metalloporphyrin catalyzed asymmetric cyclopropanation of olefins. *Tetrahedron Lett.* **1999**, *40*, 1571−1574.
(42) Du, G. D.; Andrioletti, B.; Rose, E.; Woo, L. K. Asymmetric cyclopropanation of styrene catalyzed by chiral macrocyclic iron(II) complexes. *Organometallics* **2002**, *21*, 4490−4495.
(43) Nicolas, I.; Roisnel, T.; Le Maux, P.; Simonneaux, G. Asymmetric intermolecular cyclopropanation of alkenes by diazoketones catalyzed by Halterman iron porphyrins. *Tetrahedron Lett.* **2009**, *50*, 5149−5151.
(44) Chen, Y.; Zhang, X. P. Asymmetric cyclopropanation of styrenes catalyzed by metal complexes of D_2-symmetrical chiral porphyrin: superiority of cobalt over iron. *J. Org. Chem.* **2007**, *72*, 5931−5934.
(45) Chen, Y.; Fields, K. B.; Zhang, X. P. Bromoporphyrins as versatile synthons for modular constraction of chiral porphyrins: cobalt-catalyzed highly enantioselective and diastereoselective cyclopropanation. *J. Am. Chem. Soc.* **2004**, *126*, 14718−14719.
(46) Chan, K.-H.; Guan, X.; Lo, V. K.-Y.; Che, C.-M. Elevated catalytic activity of ruthenium(II)-porphyrin-catalyzed carbene/nitrene transfer and insertion reactions with N-heterocyclic carbene ligands. *Angew. Chem., Int. Ed.* **2014**, *53*, 2982−2987.
(47) Zhou, C.-Y.; Huang, J.-S.; Che, C.-M. Ruthenium-porphyrin-catalyzed carbenoid transfer reactions. *Synlett* **2010**, *2010*, 2681−2700.
(48) Anding, B. J.; Ellern, A.; Woo, L. K. Olefin cyclopropanation catalyzed by iridium(III) porphyrin complexes. *Organometallics* **2012**, *31*, 3628−3635.
(49) Gorin, C. F.; Beh, E. S.; Bui, Q. M.; Dick, G. R.; Kanan, M. W. Interfacial electric field effect on a carbene reaction catalyzed by Rh porphyrins. *J. Am. Chem. Soc.* **2013**, *135*, 11257−11265.
(50) Simkhovich, L.; Mahammed, A.; Goldberg, I.; Gross, Z. Synthesis and characterization of germanium, tin, phosphorus, iron and rhodium complexes of tris(pentafluorophenyl)corrole, and the utilization of the iron and rhodium corroles as cyclopropanation catalysts. *Chem. - Eur. J.* **2001**, *7*, 1041−1055.
(51) Liu, H.-H.; Wang, Y.; Shu, Y.-J.; Zhou, X.-G.; Wu, J.; Yan, S.-Y. Cyclopropanation of alkenes catalyzed by metallophthalocyanines. *J. Mol. Catal. A: Chem.* **2006**, *246*, 49−52.
(52) Ventura, D. L.; Kubiak, R. W., II. Metallophthalocyanine-catalyzed cyclopropanation. *Tetrahedron Lett.* **2014**, *55*, 2715−2717.

DOI: 10.1021/acs.inorgchem.9b02718
Inorg. Chem. XXXX, XXX, XXX−XXX

(53) Sharma, V. B.; Jain, S. L.; Sain, B. Metallophthalocyanine catalyzed cyclopropanation of olefins with trimethylsilyldiazomethane: a facile and stereoselective synthesis of silylcyclopropanes. *Catal. Commun.* **2006**, *7*, 454−456.
(54) Fonseca Guerra, C.; Snijders, J. G.; te Velde, G.; Baerends, E. J. Towards an Order-N DFT Method. *Theor. Chem. Acc.* **1998**, *99*, 391−403.
(55) te Velde, G.; Bickelhaupt, F. M.; Baerends, E. J.; Fonseca Guerra, C.; van Gisbergen, S. J. A.; Snijders, J. G.; Ziegler, T. Chemistry with ADF. *J. Comput. Chem.* **2001**, *22*, 931−967.
(56) Baerends, E. J.; Ziegler, T.; Atkins, A. J.; Autschbach, J.; Bashford, D.; Bérces, A.; Bickelhaupt, F. M.; Bo, C.; Boerritger, P. M.; Cavallo, L.; et al. *ADF2016*, SCM, Theoretical ChemistryVrije Universiteit: Amsterdam, The Netherlands; https://www.scm.com.
(57) Neese, F. The ORCA Program System. *Wiley Interdiscip. Rev. Comput. Mol. Sci.* **2012**, *2*, 73−78.
(58) Neese, F. Prediction and Interpretation of the 57Fe Isomer Shift in Mössbauer Spectra by Density Functional Theory. *Inorg. Chim. Acta* **2002**, *337*, 181−192.
(59) Neese, F. Definition of Corresponding Orbitals and the Diradical Character in Broken Symmetry {DFT} Calculations on Spin Coupled Systems. *J. Phys. Chem. Solids* **2004**, *65*, 781−785.
(60) Glendening, E. D.; Landis, C. R.; Weinhold, F. NBO 6.0: Natural Bond Orbital Analysis Program. *J. Comput. Chem.* **2013**, *34*, 1429−1437.
(61) Glendening, E. D.; Badenhoop, J. K.; Reed, A. E.; Carpenter, J. E.; Bohmann, J. A.; Morales, C. M.; Landis, C. R.; Weinhold, F. *NBO 6.0*; Theoretical Chemistry Institute, University of Wisconsin: Madison, WI, 2013.
(62) Becke, A. D. Density-functional Thermochemistry. III. The Role of Exact Exchange. *J. Chem. Phys.* **1993**, *98*, 5648−5652.
(63) Grimme, S.; Antony, J.; Ehrlich, S.; Krieg, H. A Consistent and Accurate Ab Initio Parametrization of Density Functional Dispersion Correction (DFT-D) for the 94 Elements H-Pu. *J. Chem. Phys.* **2010**, *132*, 154104.
(64) Van Lenthe, E.; Baerends, E. J. Optimized Slater-type Basis Sets for the Elements 1−118. *J. Comput. Chem.* **2003**, *24*, 1142−1156.
(65) Parent, A.; Caux-Thang, C.; Signor, L.; Clemancey, M.; Sethu, R.; Blondin, G.; Maldivi, P.; Duarte, V.; Latour, J.-M. Single Glutamate to Aspartate Mutation Makes Ferric Uptake Regulator (Fur) as Sensitive to H_2O_2 as Peroxide Resistance Regulator (PerR). *Angew. Chem., Int. Ed.* **2013**, *52*, 10339−10343.
(66) Patra, R.; Coin, G.; Castro, L.; Dubourdeaux, P.; Clemancey, M.; Pecaut, J.; Lebrun, C.; Maldivi, P.; Latour, J.-M. Rational Design of Fe Catalysts for Olefin Aziridination through DFT-Based Mechanistic Analysis. *Catal. Sci. Technol.* **2017**, *7*, 4388−4400.
(67) Grimme, S.; Ehrlich, S.; Goerigk, L. Effect of the Damping Function in Dispersion Corrected Density Functional Theory. *J. Comput. Chem.* **2011**, *32*, 1456−1465.
(68) Weigend, F.; Ahlrichs, R. Balanced Basis Sets of Split Valence, Triple Zeta Valence and Quadruple Zeta Valence Quality for H to Rn: Design and Assessment of Accuracy. *Phys. Chem. Chem. Phys.* **2005**, *7*, 3297−3305.
(69) Weigend, F. Accurate Coulomb-Fitting Basis Sets for H to Rn. *Phys. Chem. Chem. Phys.* **2006**, *8*, 1057−1065.
(70) Neese, F.; Wennmohs, F.; Hansen, A.; Becker, U. Efficient, Approximate and Parallel Hartree−Fock and Hybrid DFT Calculations. A "chain-of-Spheres" Algorithm for the Hartree−Fock Exchange. *Chem. Phys.* **2009**, *356*, 98−109.
(71) Izsák, R.; Neese, F. An Overlap Fitted Chain of Spheres Exchange Method. *J. Chem. Phys.* **2011**, *135*, 144105.
(72) Klamt, A. Conductor-like Screening Model for Real Solvents: A New Approach to the Quantitative Calculation of Solvation Phenomena. *J. Phys. Chem.* **1995**, *99*, 2224−2235.
(73) English, D.; Hendrickson, D.; Suslick, K. Mössbauer spectra of Oxidized Iron Porphyrins. *Inorg. Chem.* **1983**, *22*, 367−368.
(74) Ercolani, C.; Gardini, M.; Murray, K.; Pennesi, G.; Rossi, G. Crystalline isomerism in (μ-oxo)bis[(phthalocyaninato)iron(III)]: further characterization of the isomer having a linear or quasi-linear Fe-O-Fe bond system (μ-oxo(2)). *Inorg. Chem.* **1986**, *25*, 3972−3976.
(75) Stuzhin, P. A.; Hamdush, M.; Berezin, B. D. The state of iron complexes with octaphenyl-tetraazaporphyrazine in sulfuric-acid-solutions. *Russ. J. Coord. Chem.* **1995**, *21*, 362−366.
(76) Ercolani, C.; Hewage, S.; Heucher, R.; Rossi, G. First example of a mixed-ligand bimetallic (Fe-Fe) N-bridged dimer: (μ-nitrido)[((tetraphenylporphyrinato)iron)(phthalocyaninato)iron]. *Inorg. Chem.* **1993**, *32*, 2975−2977.
(77) Ercolani, C.; Gardini, M.; Pennesi, G.; Rossi, G.; Russo, U. High-valent iron phthalocyanine μ-nitrido dimers. *Inorg. Chem.* **1988**, *27*, 422−424.
(78) Stuzhin, P. A.; Latos-Grazynski, L.; Jezierski, A. Synthesis and properties of binuclear nitride-bridged iron octaphenyltetraazaporphyrin. E.p.r. studies of dioxygen adduct formation. *Transition Met. Chem.* **1989**, *14*, 341−346.
(79) Kienast, A.; Galich, L.; Murray, K. S.; Moubaraki, B.; Lazarev, G.; Cashion, J. D.; Homborg, H. μ-Carbido diporphyrinates and diphthalocyaninates of iron and ruthenium. *J. Porphyrins Phthalocyanines* **1997**, *1*, 141−157.
(80) Soda, T.; Kitagawa, Y.; Onishi, T.; Takano, Y.; Shigeta, Y.; Nagao, H.; Yoshioka, Y.; Yamaguchi, K. Ab Initio Computations of Effective Exchange Integrals for H−H, H−He−H and Mn_2O_2 Complex: Comparison of Broken-Symmetry Approaches. *Chem. Phys. Lett.* **2000**, *319*, 223−230.
(81) Silaghi-Dumitrescu, R.; Makarov, S. V.; Uta, M.-M.; Dereven'kov, I. A.; Stuzhin, P. A. Redox non-innocence of a nitride bridge in a methane-activating dimer of iron phthalocyanine. *New J. Chem.* **2011**, *35*, 1140−1145.
(82) Lai, T.-S.; Chan, F.-Y.; So, P.-K.; Ma, D.-L.; Wong, K.-Y.; Che, C.-M. Alkene cyclopropanation catalyzed by Halterman iron porphyrin: participation of organic bases as axial ligands. *Dalton Trans.* **2006**, 4845−4861.
(83) Hansch, C.; Leo, A.; Taft, R. W. A Survey of Hammett Substituent Constants and Resonance and Field Parameters. *Chem. Rev.* **1991**, *91*, 165−195.
(84) Jiang, X.-K. Establishment and Successful Application of the $\sigma_{JJ}^{\bullet}$ Scale of Spin-Delocalization Substituent Constants. *Acc. Chem. Res.* **1997**, *30*, 283−289.
(85) Liu, J.; Hu, L.; Wang, L.; Chen, H.; Deng, L. An iron(II) ylide complex as a masked open-shell iron alkylidene species in its alkylidene-transfer reactions with alkenes. *J. Am. Chem. Soc.* **2017**, *139*, 3876−3888.
(86) Creary, X. Super radical stabilizers. *Acc. Chem. Res.* **2006**, *39*, 761−771.
(87) Creary, X.; Mehrsheikh-Mohammadi, M. E.; McDonald, S. Methylenecyclopropane rearrangement as a probe for free radical substituent efects. $\sigma^{\bullet}$ Values for commonly encountered conjugating and organometallic groups. *J. Org. Chem.* **1987**, *52*, 3254−3263.
(88) Aviv, I.; Gross, Z. Iron(III) corroles and porphyrins as superior catalysts for the reactions of diazoacetates with nitrogen- or sulfur-containing nuclephilic substrates: synthetic uses and mechanistic insights. *Chem. - Eur. J.* **2008**, *14*, 3995−4005.
(89) Khade, R. L.; Fan, W.; Ling, Y.; Yang, L.; Oldfield, E.; Zhang, Y. Iron Porphyrin Carbenes as Catalytic Intermediates: Structures, Mössbauer and NMR Spectroscopic Properties, and Bonding. *Angew. Chem., Int. Ed.* **2014**, *53*, 7574−7578.
(90) Wei, Y.; Tinoco, A.; Steck, V.; Fasan, R.; Zhang, Y. Cyclopropanations via heme carbenes: basic mechanism and effects of carbene substituent, protein axial ligand, and porphyrin substitution. *J. Am. Chem. Soc.* **2018**, *140*, 1649−1662.
(91) Coelho, P. S.; Brustad, E. M.; Kannan, A.; Arnold, F. H. Olefin cyclopropanation via carbene transfer catalyzed by engineered cytochrome P450 enzymes. *Science* **2013**, *339*, 307−310.
(92) Khade, R. L.; Zhang, Y. Catalytic and Biocatalytic Iron Porphyrin Carbene Formation: Effects of Binding Mode, Carbene Substituent, Porphyrin Substituent, and Protein Axial Ligand. *J. Am. Chem. Soc.* **2015**, *137*, 7560−7563.

DOI: 10.1021/acs.inorgchem.9b02718
Inorg. Chem. XXXX, XXX, XXX−XXX

(93) Sharon, D. A.; Mallick, D.; Wang, B.; Shaik, S. Computation Sheds Insight into Iron Porphyrin Carbenes' Electronic Structure, Formation, and N−H Insertion Reactivity. *J. Am. Chem. Soc.* **2016**, *138*, 9597−9610.
(94) Khade, R. L.; Zhang, Y. C−H Insertions by Iron Porphyrin Carbene: Basic Mechanism and Origin of Substrate Selectivity. *Chem. - Eur. J.* **2017**, *23*, 17654−17658.
(95) Aldajaei, J. T.; Gronert, S. The Gas-Phase Reactions of Metal Porphyrins with Diazoacetate Esters. *Int. J. Mass Spectrom.* **2012**, *316-318*, 68−75.
(96) Wang, H.-X.; Wan, Q.; Wu, K.; Low, K.-H.; Yang, C.; Zhou, C.-Y.; Huang, J.-S.; Che, C.-M. Ruthenium(II) porphyrin quinoid carbene complexes: synthesis, crystal structure, and reactivity toward carbene transfer and hydrogen atom transfer reactions. *J. Am. Chem. Soc.* **2019**, *141*, 9027−9046.
(97) Sorokin, A. B. Recent progress on exploring μ-oxo bridged binuclear porphyrinoid complexes in catalysis and material science. *Coord. Chem. Rev.* **2019**, *389*, 141−160.
(98) Zhang, Y. Computational investigations of heme carbenes and heme carbene transfer reactions. *Chem. - Eur. J.* **2019**, *25*, 13231−13247.
(99) Torrent-Sucarrat, M.; Arrastia, I.; Arrieta, A.; Cossio, F. P. Stereoselectivity, different oxidation states, and multiple spin states in the cyclopropanation of olefins catalyzed by Fe-porphyrin complexes. *ACS Catal.* **2018**, *8*, 11140−11153.
(100) Su, H.; Ma, G.; Liu, Y. Theoretical insights into the mechanism and stereoselectivity of olefin cyclopropanation catalyzed by two engineered cytochrome P450 enzymes. *Inorg. Chem.* **2018**, *57*, 11738−11745.

DOI: 10.1021/acs.inorgchem.9b02718
Inorg. Chem. XXXX, XXX, XXX−XXX